Current Pharmaceutical Analysis 22 (2026) 10–22

Contents lists available at ScienceDirect

Current Pharmaceutical Analysis

journal homepage: www.keaipublishing.com/en/journals/cpa/

Full Length Article

Immunomodulatory and skin-compatible effects of *Amaranthus retroflexus* volatile compounds: An *in-silico* network and pathway-based approach

Erdi Can Aytar[a,*], Abidin Gümrükçüoğlu[b], Emine Incilay Torunoğlu[c], Saleh Al-Farraj[d], Mika Sillanpää[e,f,**]

[a] *Usak University Faculty of Agriculture Department of Horticulture, Uşak 64200, Turkey*
[b] *Artvin Çoruh University, Medicinal-Aromatic Plants Application and Research Center, Artvin 08000, Turkey*
[c] *Necmettin Erbakan University, Faculty of Medicine, Department of Medical Biochemistry, Konya 42090, Turkey*
[d] *Department of Zoology, College of Science, King Saud University, Riyadh 11451, Saudi Arabia*
[e] *Institute of Research and Development, Duy Tan University, Da Nang 550000, Viet Nam*
[f] *School of Engineering & Technology, Duy Tan University, Da Nang 550000, Viet Nam*

ARTICLE INFO

Keywords:
Bioactivity prediction
Endocrine disruption
Fatty acid esters
GC-MS analysis
In silico modeling
Squalene
Skin sensitization

ABSTRACT

Background: This study investigated the phytochemical profile, in silico skin sensitization, cosmetic toxicity, and endocrine-disrupting potential of compounds from *Amaranthus retroflexus* identified through GC-MS analysis.
Methods: Volatile constituents were identified using gas chromatography–mass spectrometry (GC–MS) analysis. The safety profiles of the major compounds were evaluated through *in silico* toxicity prediction models, including keratinosens, local lymph node assay (LLNA) and human cell line activation test (h-CLAT), along with molecular docking analysis to assess their endocrine-disrupting potential.
Results: A total of 39 distinct compounds were identified, with a predominant presence of unsaturated fatty acid methyl esters, including 9,12-octadecenoic acid, methyl ester (47.275 %) and 9-octadecenoic acid, methyl ester (22.790 %). Other notable compounds included methyl stearate (3.063 %), Squalene (9.687 %), and various alkanes. *In silico* skin sensitization analysis demonstrated that all five key compounds, including hexadecenoic acid methyl ester, methyl stearate, and squalene, fell within the applicability domain of the predictive models. High predictive confidence was observed in both the KeratinoSens and LLNA models, whereas the h-CLAT model exhibited lower predictive reliability. Cosmetic toxicity predictions revealed moderate to high risks for skin and eye irritation, particularly with Squalene, but the compounds were considered safe regarding systemic toxicity and photo-related effects. Furthermore, endocrine-disrupting potential was evaluated via *in silico* binding affinity analysis, which revealed minimal interaction with nuclear receptors.
Conclusion: These findings highlight the potential of the plant extract for dermatological applications, while emphasizing the need for further evaluation of its safety in topical use.

Abbreviation: ADMETlab 3.0, Absorption, Distribution, Metabolism, Excretion, and Toxicity laboratory, in silico platform; AR, Androgen Receptor; AR-an, Androgen Receptor antagonist; CLUE.io, Connectivity Map platform; CYP1A1, Cytochrome P450 1A1; DPRA, Direct Peptide Reactivity Assay; FDR, False Discovery Rate; GC-MS, Gas Chromatography–Mass Spectrometry; GR, Glucocorticoid Receptor; GSTP1, Glutathione S-transferase Pi 1; HRIPT/HMT, Human Repeat Insult Patch Test / Human Maximization Test; HMOX1, Heme Oxygenase 1; IL10, Interleukin 10; IL6, Interleukin 6; KEAP1, Kelch-like ECH-associated protein 1; KEGG, Kyoto Encyclopedia of Genes and Genomes; LE, Ligand Efficiency; LINCS L1000, Library of Integrated Network-based Cellular Signatures; LLNA, Local Lymph Node Assay; LLE, Lipophilic Ligand Efficiency; MAPK1, Mitogen-Activated Protein Kinase 1; MVD, Molegro Virtual Docker; NFE2L2, Nuclear factor erythroid 2–related factor 2; PDB, Protein Data Bank; PKA, Protein Kinase A; PPAR, Peroxisome Proliferator-Activated Receptor; PPI, Protein–Protein Interaction network; PIC_{50}, Negative logarithm of the half-maximal inhibitory concentration; Pred-Skin 3.0, *In silico* skin sensitization prediction platform; RXR, Retinoid X Receptor; Squalene, Plant-derived triterpenoid hydrocarbon; TPSA, Topological Polar Surface Area; TNF, Tumor Necrosis Factor; TR, Thyroid Receptor

* Corresponding author.
** Corresponding author at: Institute of Research and Development, Duy Tan University, Da Nang, Viet Nam.
E-mail addresses: erdi.aytar@usak.edu.tr (E.C. Aytar), mikaetapiosillanpaa@duytan.edu.vn (M. Sillanpää).

https://doi.org/10.1016/j.cpan.2025.11.005
Received 12 September 2025; Received in revised form 28 November 2025; Accepted 30 November 2025
Available online 1 December 2025

1. Introduction

Amaranthus retroflexus L. (Redroot pigweed) is a commonly encountered species belonging to the Amaranthaceae (amaranth family) [1]. This plant is a member of the *Amaranthus* genus. *A. retroflexus* is a flowering annual species and is commonly referred to by various names such as redroot amaranth, redroot pigweed, common amaranth, and pigweed amaranth [2]. It is distributed across the European part of Russia, Siberia, Southern Europe, the Middle East, Asia Minor, Mongolia, and North Africa [3]. Amaranth leaves are widely used both in cooked dishes and in salads. *Amaranthus* is highly nutritious and contains higher levels of protein and minerals compared to commonly consumed grains such as millet, sorghum, rice, wheat, and maize. Moreover, it has a well-balanced composition of essential amino acids and unsaturated fatty acids [4]. Although *A. retroflexus* may exhibit toxic effects on animals when consumed raw or in large quantities, it can be safely used as a vegetable or forage when properly processed.

Essential oils are used as flavoring agents in the food industry, with approximately 300 different types commercially available [5]. The antimicrobial properties of these compounds have led to their consideration as natural preservative agents [6]. However, research on the biological effects of essential oils on human skin cells remains limited [7]. Essential oils are complex natural mixtures derived from aromatic plants, typically composed of low molecular weight compounds such as monoterpenes, sesquiterpenes, and aliphatic hydrocarbons. These oils are widely used in topical applications, aromatherapy, cosmetics, and traditional medicine. However, upon direct contact with the skin, they have the potential to cause irritation, allergic reactions, or immunotoxic effects [8–10].

With the growing interest in natural formulations, global demand for beauty and personal care products has increased. However, the cost and limited availability of natural compounds have led to the widespread use of synthetic alternatives. While skin aging is accelerated by environmental factors, antioxidants play a crucial role in mitigating this damage; in particular, phenolic compounds hold potential in regulating melanin synthesis and preventing various diseases [11].

In a study conducted by Han et al. [12] the biological activities of nine plant-derived essential oils and a commercial “Immortelle” blend were investigated in human dermal fibroblast cells pretreated to mimic chronic inflammatory conditions. The study evaluated bergamot, coriander, geranium, helichrysum, patchouli, petitgrain, sandalwood, vetiver, ylang ylang, and the Immortelle blend. All oils significantly suppressed fibroblast proliferation; notably, bergamot, coriander, and vetiver oils were found to reduce protein levels associated with inflammation, immune response, and tissue repair. Helichrysum, ylang ylang, and the Immortelle blend were also suggested to exert potential anti-inflammatory and wound-healing effects by downregulating the expression of proteins involved in tissue regeneration.

Topical drug administration offers advantages over oral delivery, such as improved patient compliance, avoidance of first-pass metabolism, and the ability to deliver the active compound directly to the target site. However, skin barriers such as the epidermis, dermis, and hypodermis limit the dermal penetration of formulations [13]. Natural oils have long been used due to their therapeutic efficacy and low side effect profiles. Nevertheless, the biological effects and potential toxicities of these compounds in topical applications are often insufficiently investigated. While the beneficial effects of herbal medicines are widely acknowledged, uncontrolled and ethnopharmacology-based applications may lead to serious health issues, even in traditionally used species [11]. For example, the misuse of *Aristolochia* species—once considered of high medicinal value—has resulted in numerous cases of end-stage renal disease due to aristolochic acid toxicity; many patients developed nephropathy requiring organ transplantation or dialysis [14,15].

In this study, the fatty acid composition of *Amaranthus retroflexus* L. was characterized by GC-MS analysis, and the dermal safety profile of this composition was evaluated using *in silico* methods. To determine the chemical profile of fatty acids, FAME analysis, an internationally standardized method, was employed. The obtained fatty acid profile (carbon chain length, degree of unsaturation) reflects the structural properties of the raw plant oil, and this information is valuable for both fundamental research and cosmetic/dermatological formulation development. The fundamental value of the study lies in providing detailed characterization of the plant's lipid content; its practical value is that the dermal safety and bioactivity potential of the identified fatty acids and squalene are evaluated through *in silico* methods, thereby guiding future *in vitro* and *in vivo* studies. Gas chromatography-mass spectrometry (GC-MS) analysis of the oil obtained from the selected plant species identified hexadecenoic acid, methyl ester, methyl stearate, 9-octadecenoic acid, methyl ester, 9,12-octadecenoic acid, methyl ester, and Squalene as the major components. These compounds, structurally classified as fatty acid methyl esters and triterpenoid derivatives, are widely recognized in the literature for their antioxidant, anti-inflammatory, and dermal biocompatibility properties. However, the potential immunotoxic effects of such natural compounds in topical applications should not be overlooked.

2. Materials and methods

2.1. Plant materials

The above-ground parts of *A. retroflexus* were dried at 40 °C for 72 h. The dried plant material was then mixed with methanol in a 1:10 ratio and macerated in a dark environment at room temperature for two days. After extraction, the methanol (Catalog No.: 848335, Sigma-Aldrich, St. Louis, MO, USA) solution was filtered through Whatman No. 1 filter paper (Whatman International Ltd., Maidstone, UK). The solvent was then evaporated under reduced pressure using a rotary evaporator (Model: RE100, Stuart, Staffordshire, UK) at 40°C. The resulting solid extracts were stored at 4 °C for further analysis [16].

2.2. Fatty acid extraction and GC-MS analysis protocol

For the extraction of fatty acids, 5 g of dried and finely ground plant material were processed using a laboratory mill. The pulverized sample was placed into a cellulose extraction thimble and subjected to Soxhlet extraction utilizing a fully automated Soxhlet system. Hexane (Catalog No.: 139386, Sigma-Aldrich, St. Louis, MO, USA) was employed as the extraction solvent over a 4-hour period. After completion, the solvent was removed by rotary evaporation, and the resulting oil was collected in clean glass vials for derivatization.

To convert fatty acids into their corresponding methyl esters, 0.1 g of the extracted oil was transferred into a 5 mL reaction vial. Next, 2 mL of n-hexane was added, and the contents were mixed using a vortex mixer. Then, 0.2 mL of 2 N methanol KOH (Catalog No.: 221 473, Sigma-Aldrich, St. Louis, MO, USA) was introduced. The tube was sealed and shaken vigorously for 30 s to ensure transesterification. Following a brief centrifugation (Model: 3–16 KC, Sigma Laborzentrifugen GmbH, Osterode am Harz, Germany) step to promote phase separation, the upper (organic) phase containing fatty acid methyl esters (FAMEs) was carefully collected using a Pasteur pipette and transferred into GC vials.

Chromatographic analysis was performed using a gas chromatography system (Agilent Technologies, Santa Clara, CA, USA) coupled to a mass spectrometer, equipped with an HP-88 capillary column (60 m × 0.25 mm ID × 0.20 μm film thickness, Agilent Technologies, Santa Clara, CA, USA). Helium, with a purity greater than 99.99 %, served as the carrier gas at a steady flow rate of 1.0 mL/min. The oven temperature program began at 140 °C with a 5-minute hold, followed by a ramp of 4 °C/min to a final temperature of 250 °C, which was then maintained for 10 min. A sample volume of 1 μL was injected in split mode at a ratio of 1:50.

Mass spectrometric detection was carried out in electron impact (EI) ionization mode at 70 eV. The ion source temperature was maintained at 230 °C, and spectra were recorded within a mass-to-charge (*m/z*) range of 30–550. Fatty acid methyl esters were identified by comparing retention times and mass spectra with the Supelco 37 Component FAME Mix standard (Sigma-Aldrich, St. Louis, MO, USA). Retention Index (RI) values were calculated using this standard mixture to confirm compound identities and exclude peak overlap.

2.3. AOP-based approach for skin sensitization assessment

In this study, the potential immunological responses and toxic effects of plant-derived natural compounds upon dermal exposure were systematically evaluated within an Adverse Outcome Pathway (AOP)-based framework. Specifically, predictive computational models aligned with the in vitro and in chemico test strategies recommended by the OECD were employed to assessthe risk of potential skin sensitization.

In the initial phase, the skin sensitization profiles of the selected compounds were determined using the Pred-Skin 3.0 platform. This platform provides *in silico* simulations corresponding to key OECD test guidelines, including OECD TG 442 C (Direct Peptide Reactivity Assay – DPRA), OECD TG 442D (KeratinoSens™ assay), OECD TG 442E (Human Cell Line Activation Test – h-CLAT), and OECD TG 429 (Local Lymph Node Assay – LLNA). Each compound was classified as either a "Sensitizer" or "Non-sensitizer" at individual assay levels. A final sensitization prediction was generated using a probabilistic Bayesian integration model that combines results from these mechanistic stages.

2.4. In silico cosmetic risk and toxicity assessment (ADMETlab 3.0)

In this study, the cosmetic safety and toxicity profiles of five major volatile constituents—hexadecenoic acid, methyl ester; methyl stearate; 9-octadecenoic acid, methyl ester; 9,12-octadecenoic acid, methyl ester; and Squalene—were evaluated using the in-silico platform ADMET lab 3.0 (https://lmmd.ecust.edu.cn/admetsar3/predict.php). The analysis focused on key safety endpoints relevant to topical and dermal exposure, including eye corrosion, eye irritation, skin corrosion, skin irritation, skin sensitization, acute dermal toxicity, photoinduced toxicity, phototoxicity, and photoallergy. For each compound, the platform provided a binary risk classification (Yes/No) along with a probability score (%) for each endpoint, based on machine learning models trained on curated experimental datasets. All inputs were submitted in canonical SMILES format, and predictions were generated under standard model settings. The obtained data allowed for a comparative evaluation of potential risks associated with the dermal and ocular application of the compounds. Special attention was given to endpoints with high-confidence predictions (probability > 70 %), to support a preliminary toxicological assessment of these plant-derived molecules for cosmetic or dermatological formulations.

2.5. In silico evaluation of endocrine disruption potential

The potential endocrine-disrupting effects of the five major volatile constituents identified by GC-MS analysis—hexadecenoic acid, methyl ester, methyl stearate, 9-octadecenoic acid, methyl ester, 9,12-octadecenoic acid, methyl ester, and Squalene—were assessed using the Endocrine Disruptome web-based platform (http://endocrinedisruptome.ki.si/). This computational tool employs molecular docking algorithms to predict the binding affinity of small molecules toward a panel of 15 human nuclear hormone receptors, including estrogen receptors (ERα, ERβ), androgen receptors (AR, AR-an), glucocorticoid receptor (GR), thyroid receptors (TRα, TRβ), progesterone receptor (PR), mineralocorticoid receptor (MR), liver X receptors (LXRα, LXRβ), peroxisome proliferator-activated receptors (PPARα, PPARβ, PPARγ), and retinoid X receptor (RXRα).

The evaluation was conducted by submitting the SMILES codes of each compound into the system. Predictions were generated based on binding scores derived from AutoDock Vina algorithms, and results were visualized using a color-coded probability scheme: green for low, yellow for moderate, and red for high binding affinity. Each compound's interaction profile with individual receptors was recorded and interpreted with respect to its potential to act as an agonist or antagonist. Compounds displaying moderate to high affinity to key endocrine receptors, particularly ERα, AR, and PPARs, were flagged for potential concern. The outputs were analyzed in relation to the biological relevance of the targets and integrated into the overall safety assessment framework of the plant extract studied.

2.6. Construction of a skin-associated gene set

In parallel with the biological activity predictions obtained from Pred-Skin analyses, genes associated with cutaneous immune responses were identified based on the Adverse Outcome Pathway (AOP) knowledge base, comprehensive literature reviews, and particularly the molecular initiating events and key events outlined in OECD TG 442E guidelines.

Within this framework, a total of 25 target genes were selected for their involvement in fundamental mechanisms such as stress response, cytokine production, T cell activation, and apoptosis in skin cells. The selected genes include key immune, inflammatory, and metabolic regulators such as TNF, IL6, STAT1, RELA, MAPK1, CYP1A1, CYP1B1, HMOX1, NFE2L2, KEAP1, CD86, and CASP3, all of which encode proteins with critical roles in skin-related immunological processes.

2.7. Protein-protein interaction (PPI) network and string-based analysis

The identified genes were subjected to protein-protein interaction (PPI) network analysis using the STRING database (https://string-db.org/). The resulting interaction data file (string_interactions_short.tsv) was imported into the Cytoscape platform (version 3.9.1) and visualized using the Prefuse Force Directed layout algorithm.

Key topological parameters of the network—including the number of nodes and edges, network diameter, density, clustering coefficient, and degree distribution—were calculated. Central (hub) genes within the network were identified based on their degree and betweenness centrality values, providing insight into their potential regulatory importance in skin-related immune pathways.

2.8. Functional and proportional analysis of KEGG pathways (ClueGO)

To investigate the functional distribution of genes within the PPI network, a KEGG-based pathway enrichment analysis was performed using the ClueGO plugin (v2.5.10). The analysis was conducted for *Homo sapiens* (Taxonomy ID: 9606), and only ontological terms supported by experimental evidence codes (e.g., EXP, IDA, IMP) were included. A p-value threshold of 0.01 was applied, and a minimum of 40 % shared genes was set as the criterion for pathway clustering. The visualization was performed using the "Groups" style layout, with distinguishable color codes assigned to each pathway group. The pie chart mode was disabled in favor of node-based color smoothing to enhance clarity, and hub pathways were highlighted based on their topological relevance.

In addition, the KEGG pathways identified through ClueGO were proportionally evaluated using the platform's automatically generated pie chart. This graphical representation illustrates the relative contribution of gene clusters to each biological pathway, allowing for a visual interpretation of the dominant functional categories. The proportional analysis provided insights into which biological processes were most significantly associated with the tested compounds, emphasizing their involvement in specific dermal immunological and inflammatory mechanisms.

2.9. Molecular docking

TNF (PDB ID: 2AZ5) was selected as a primary docking target, as it is a key component of the Th17 cell differentiation pathway—identified as the most enriched module in the ClueGO analysis—and also emerged as the top hub protein in the constructed protein-protein interaction (PPI) network. In the KEGG analysis, TNF was highlighted as a central initiator of immune responses, cytokine production, and inflammatory signaling, particularly triggering T cell polarization following dendritic cell activation in the skin. Due to its central role in both the KEGG and PPI networks and its high-resolution crystal structure, TNF was prioritized for docking studies related to skin sensitization.

MAPK1 (PDB ID: 2ZOQ) is a multifunctional signaling protein intersecting not only with the Inflammatory Bowel Disease (IBD) pathway but also with Th17 cell differentiation and Fluid shear stress modules. Its extensive interactions with other genes within the PPI network position it as a critical signaling node. Moreover, its regulatory role in transmitting signals from cytokines such as IL-6 and TNF in epidermal cells makes it a relevant target in skin-related immune signaling and thus a candidate for molecular docking.

HMOX1 (PDB ID: 1N3U) was specifically associated with the Fluid shear stress and atherosclerosis pathway according to ClueGO analysis. It plays a protective role in the epidermal stress response and oxidative damage regulation. Within the STRING network, it forms strong connections particularly with KEAP1 and NFE2L2, contributing to redox homeostasis. Due to its pathway-specific role and high-quality crystal structure, HMOX1 was selected as a docking target to model dermal oxidative stress responses.

CYP1A1 (PDB ID: 4I8V), although more peripheral in the ClueGO network, is functionally critical within the Chemical carcinogenesis pathway. It is a key metabolic enzyme involved in the oxidative biotransformation of skin-absorbed xenobiotics and plays an essential role in converting potential sensitizers into reactive intermediates. Its clearly defined binding pocket and bridging function within metabolic processes in the KEGG-PPI network justify its inclusion as a target in the docking simulations.

Molecular docking studies were conducted to assess the binding affinities and interaction profiles of major plant-derived metabolites identified through GC-MS analysis. The compounds tested included hexadecanoic acid, methyl ester, methyl stearate, 9-octadecenoic acid, methyl ester, 9,12-octadecenoic acid, methyl ester, and Squalene. These molecules, primarily fatty acid methyl esters and a triterpenoid, are well-documented in the literature for their anti-inflammatory, antioxidant, and skin-compatible properties.

The three-dimensional (3D) structures of these ligands were retrieved from the PubChem database and subjected to energy minimization to ensure optimal geometry and conformational stability prior to docking. For docking simulations, biologically relevant protein targets were obtained from the RCSB Protein Data Bank, including 2AZ5 (TNF-α with inhibitor), 2ZOQ (ERK1), 1N3U (heme oxygenase 1), and 4I8V (cytochrome P450 1A1).

Protein structures were prepared using AutoDock Tools (v1.5.7) by removing crystallographic water molecules and non-standard ligands, adding polar hydrogen atoms, and assigning Gasteiger partial charges. Docking was carried out using AutoDock Vina, with grid boxes precisely defined to encompass the active sites of the target proteins. Multiple conformations were generated for each ligand, and the pose with the lowest binding free energy (kcal/mol) was selected for further analysis.

For detailed interaction mapping, the best docking poses were analyzed using Molegro Virtual Docker (MVD) to identify critical interactions such as hydrogen bonding, van der Waals forces, electrostatic interactions, and spatial accommodation within the active site cavities. Cavity detection and scoring facilitated a nuanced understanding of ligand orientation and binding affinity. Final three-dimensional visualizations were performed using Discovery Studio Visualizer (v21.1.0) to examine ligand–protein interactions and pinpoint key amino acid residues involved in molecular recognition, thereby supporting the interpretation of structure–activity relationships [17].

2.10. Connectivity map (CLUE.io) and LINCS L1000 analysis

In this study, the biological effects of Squalene, the compound exhibiting the highest binding affinity to the target protein CYP1A1 in molecular docking analyses, were evaluated using advanced systems biology approaches. Specifically, *in silico* gene expression profiling and pathway analyses were conducted to explore the broader molecular implications.

In the initial step, CRISPR-based knockout data for the CYP1A1 gene were queried using the CLUE.io platform. The dataset utilized was derived from the LINCS L1000 CMAP Consensus Signatures collection. As a result of this query, 476 genes were identified as upregulated in response to CYP1A1 gene silencing.

This gene expression signature was employed as a foundational dataset for subsequent biological network analyses, aiming to model the indirect effects of compounds—particularly Squalene—that demonstrate strong binding affinity to the CYP1A1 protein.

2.11. Reactome pathway enrichment analysis

The list of upregulated genes was analyzed using the Reactome Pathway Browser to identify biologically meaningful pathways. Pathways with a False Discovery Rate (FDR) below 0.05 were considered statistically significant and selected for further evaluation. Among the enriched pathways, two were highlighted for their strong biological relevance. The first, PKA activation in glucagon signalling (R-HSA-164952), is closely associated with cellular energy metabolism, the activation of protein kinase A (PKA), and the regulation of anti-inflammatory cytokines such as IL6 and IL10. The second pathway, Differentiation of Keratinocytes in Interfollicular Epidermis (R-HSA-9725554), is critical for maintaining epidermal homeostasis, promoting keratinocyte maturation, and supporting dermal barrier integrity. These two pathways were further investigated to provide insight into the potential systemic (metabolic) and local (epidermal) effects of Squalene, particularly in the context of its high-affinity interaction with CYP1A1. High-resolution graphical diagrams of the identified pathways were obtained from the Reactome Pathway Browser interface and archived in a publication-ready format. These pathway maps visually highlighted the positions of the upregulated genes within each pathway, thereby supporting the mechanistic interpretation of the results.

3. Result

3.1. GC-MS-based phytochemical profile

As a result of GC-MS analysis, a total of 39 distinct compounds were identified in the plant extract, including various saturated and unsaturated fatty acid methyl esters, alkanes, and triterpenoid constituents. These compounds were evaluated based on both their relative abundance and structural characteristics (Table 1).

The composition was predominantly composed of unsaturated fatty acid methyl esters. Among these, 9,12-octadecenoic acid, methyl ester (47.275 %) and 9-octadecenoic acid, methyl ester (22.790 %) was identified as the most abundant constituents. These were followed by Methyl stearate (3.063 %), linolenic acid, methyl ester (1.093 %), and eicosanoic acid, methyl ester (1.025 %), representing long-chain saturated and polyunsaturated fatty acid derivatives. Given their well-documented anti-inflammatory, antioxidant, and skin-compatible properties, these compounds offer significant insight into the potential bioactivity of the extract.

In addition, the extract contained Squalene at a notable concentration of 9.687 %. This plant-derived triterpenoid is widely recognized for

Table 1
Identified compounds and their relative abundance in the plant extract (GC-MS).

No	RT (min)	RI	Name of the compound	Content [%]
1	5.543	715	Tetradecane	0.014
2	6.364	906	Hexadecane	0.006
3	9.985	1396	Dodecanoic acid, methyl ester	0.003
4	13.081	1448	Methyl tetradecanoate	0.080
5	14.257	1496	Methyl 12-methyltetradecanoate	0.014
6	14.771	1588	Pentadecanoic acid, methyl ester	0.034
7	15.625	1647	Methyl 14-methylpentadecanoate	0.013
8	16.649	1707	Hexadecanoic acid, methyl ester	10.332
9	17.359	1749	Methyl palmitelaidate;	0.208
10	17.680	1769	Methyl 14-methylhexadecanoate	0.424
11	18.180	1799	Heptadecanoic acid, methyl ester	0.064
12	18.643	1827	(*Z*)-Methyl Heptadec-10-enoate	0.007
13	18.704	1827	7,10-hexadecadienoic acid	0.007
14	19.108	1855	Heptadecanoic acid, 15-methyl-,methyl ester	0.737
15	20.291	1915	Methyl stearate	3.063
16	20.979	1937	9-Octadecenoic acid, methyl ester	22.790
17	21.069	1940	7-Octadecenoic acid, methyl ester	0.949
18	21.271	1946	Nonadecanoic acid, methyl ester	0.153
19	21.457	1952	Oleic acid, methyl ester	0.027
20	21.823	1965	17-Octadecynoic acid, methyl ester	0.041
21	22.428	1984	9,12-Octadecenoic acid, methyl ester	47.275
22	22.987	2104	Eicosanoic acid, methyl ester	1.025
23	23.559	2144	Linolenic acid, methyl ester	1.093
24	23.775	2159	cis-Methyl 11-eicosenoate	0.324
25	23.970	2172	Glycerin	0.473
26	24.099	2181	Octacosane	0.063
27	24.380	2200	Heneicosanoic acid, methyl ester	0.088
28	24.680	2222	1-Octadecene	0.036
29	24.726	2225	1-Heptadecene	0.026
30	25.009	2245	11,14-Eicosadienoic acid, methyl ester	0.076
31	25.761	2299	Docosanoic acid, methyl ester	0.243
32	26.540	2357	13-Docosenoic acid, methyl ester, (*Z*)-	0.012
33	26.700	2369	Methyl 20-methyl-docosanoate	0.024
34	26.821	2378	Octadecane	0.048
35	27.257	2411	Squalene	9.687
36	27.987	2467	3-Methylhentriacontane	0.040
37	28.415	2500	Tetracosanoic acid, methyl ester	0.133
38	29.3	2532	Methyl 17-methyl-tetracosanoate	0.035
39	30.209	2565	Hexacosanoic acid, methyl ester	0.015
			Total%	99.7

its high bioavailability and potent antioxidant capacity, along with beneficial effects on skin health, making it a compound of considerable interest. Minor constituents such as tetradecane, hexadecane, octadecane, and 3-methylhentriacontane classified as alkanes are likely inert hydrocarbons that may have been co-extracted due to solvent affinity during the extraction process.

In conclusion, the high abundance of unsaturated fatty acid methyl esters and squalene supports the potential application of the plant extract as an anti-inflammatory, emollient, and moisturizing agent in dermatological formulations.

3.2. *In silico findings on skin sensitization*

In silico analyses performed using the Pred-Skin 3.0 platform revealed that all five tested compounds—hexadecanoic acid, methyl ester, methyl stearate, 9-octadecenoic acid, methyl ester, 9,12-octadecenoic acid, methyl ester, and Squalene—were classified as falling within the applicability domain of all predictive models (Table 2, Fig. 1).

In the DPRA (Direct Peptide Reactivity Assay) model, all compounds were evaluated within the model's domain, with confidence levels ranging from 50.8 % to 92.5 %, indicating a reliable prediction performance. Similarly, in the KeratinoSens model, all compounds were again within the applicability domain, with particularly high confidence scores for 9-Octadecenoic acid, methyl ester (96.5 %), 9,12-Octadecenoic acid, methyl ester (96.4 %), and Squalene (97.4 %).

In contrast, the h-CLAT (Human Cell Line Activation Test) model yielded lower confidence scores for all compounds (ranging from 56.4 % to 59.2 %), suggesting relatively lower predictive certainty in this assay compared to others.

The Local Lymph Node Assay (LLNA) model indicated very high confidence for methyl stearate (99.7 %), 9-octadecenoic acid, methyl ester (99.8 %), and Squalene (99.9 %), while hexadecanoic acid, methyl ester and 9,12-octadecenoic acid, methyl ester showed moderate confidence scores of 55.6 % and 65.4 %, respectively.

Within the Human Repeat Insult Patch Test / Human Maximization Test (HRIPT/HMT) model, all compounds except hexadecanoic acid, methyl ester were located within the applicability domain, with confidence values ranging from 69.8 % to 97.0 %. hexadecanoic acid, methyl ester was the only compound found outside the domain for this model.

Importantly, all five compounds received a "High" overall confidence rating from the Bayesian integration model, indicating a strong predictive reliability and suggesting a low potential for skin sensitization under the evaluated conditions.

3.3. *In silico cosmetic toxicity predictions*

In this study, the cosmetic safety profiles of five major compounds identified through GC-MS—hexadecenoic acid, methyl ester, methyl stearate, 9-octadecenoic acid, methyl ester, 9,12-octadecenoic acid, methyl ester, and Squalene—were evaluated using the *in-silico* platform ADMETlab 3.0. The assessment focused on nine key dermal and ocular

Table 2
In Silico skin sensitization predictions and model confidence scores for selected compounds (Pred-Skin 3.0).

Test / Evaluation	Hexadecanoic acid, methyl ester	Methyl stearate	9-Octadecenoic acid, methyl ester	9,12-Octadecenoic acid, methyl ester	Squalene
DPRA AD	Inside	Inside	Inside	Inside	Inside
DPRA Confidence (%)	88.30	88.30	89.10	50.80	92.50
DPRA AD Probability map	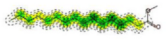				
KeratinoSens AD	Inside	Inside	Inside	Inside	Inside
KeratinoSens Confidence (%)	88.00	88.00	96.50	96.40	97.40
KeratinoSens AD Probability map	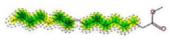		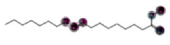		
h-CLAT AD	Inside	Inside	Inside	Inside	Inside
h-CLAT Confidence (%)	58.30	58.30	56.40	56.40	59.20
h-CLAT AD Probability map	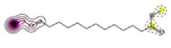	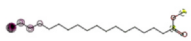	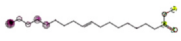	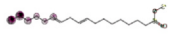	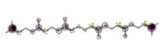
LLNA AD	Inside	Inside	Inside	Inside	Inside
LLNA Confidence (%)	55.60	99.70	99.80	65.40	99.90
LLNA AD Probability map		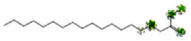	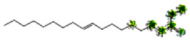		
HRIPT/HMT AD	Outside	Inside	Inside	Inside	Inside
HRIPT/HMT Confidence (%)	97.00	97.00	83.40	69.80	70.30
HRIPT/HMT AD Probability map	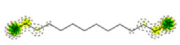	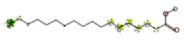		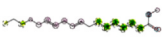	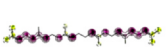
Bayesian Confidence	High	High	High	High	High

toxicity endpoints relevant to cosmetic applications: eye corrosion, eye irritation, skin corrosion, skin irritation, skin sensitization, acute dermal toxicity, photoinduced toxicity, phototoxicity, and photoallergy (Table 3, Supplementary Information Figure S-1).

The results indicated that all compounds were predicted to pose a risk for eye corrosion (probabilities ranging from 59.4 % to 95.8 %) and eye irritation (87.5–98.6 %). In contrast, all compounds were classified as non-corrosive to skin, with low probability scores (23.5–35.3 %). For

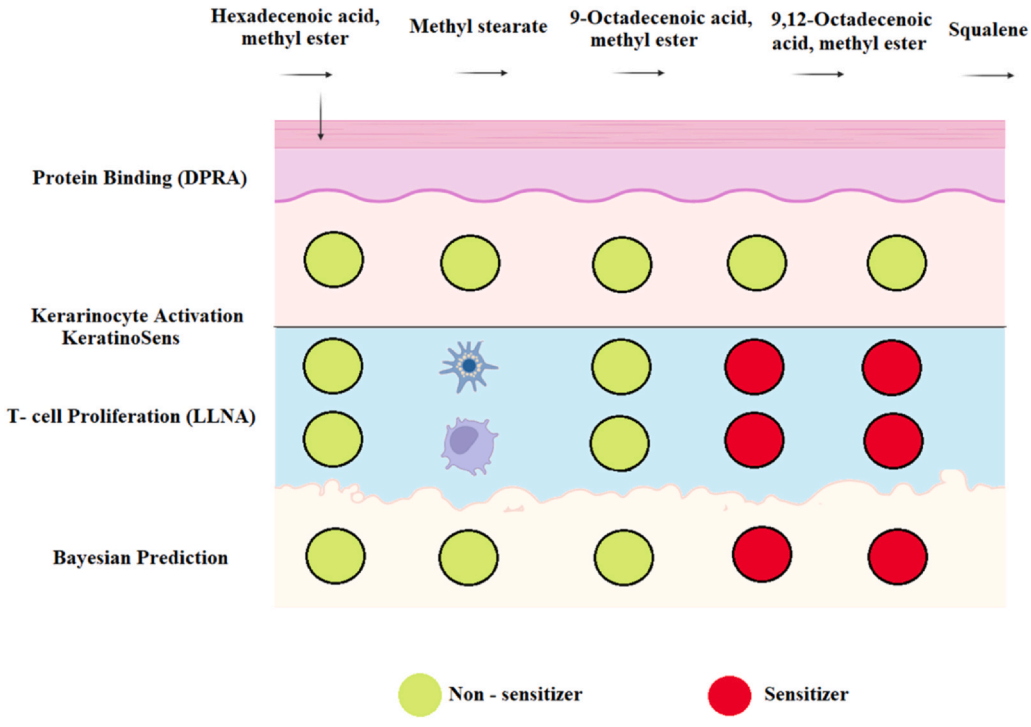

Fig. 1. *In silico* skin sensitization predictions of major compounds based on DPRA, KeratinoSens, LLNA, and Bayesian model (created by Emine İncilay Torunoğlu via BioRender).

Table 3
Cosmetic risk assessment and toxicity predictions of major component.

Cosmetic Risk Assessment	Hexadecenoic acid, methyl ester		Methyl stearate		9-Octadecenoic acid, methyl ester		9,12-Octadecenoic acid, methyl ester		Squalene	
	Risk (Yes/No)	Probability (%)	Risk (Yes/No)	Probability (%)	Risk (Yes/No)	Probability (%)	Risk (Yes/No)	Probability (%)	Risk (Yes/No)	Probability (%)
Eye corrosion	Yes	95.80	Yes	92.40	Yes	89.60	Yes	82.20	Yes	59.40
Eye irritation	Yes	98.60	Yes	97.50	Yes	97.90	Yes	97.80	Yes	87.50
Skin corrosion	No	35.00	No	35.30	No	30.50	No	23.50	No	24.80
Skin irritation	Yes	60.30	Yes	52.10	Yes	58.20	Yes	63.40	Yes	70.70
Skin sensitisation	Yes	76.30	Yes	69.09	Yes	75.70	Yes	81.00	Yes	84.30
Acute dermal toxicity	No	23.80	No	37.10	No	27.30	No	18.20	No	33.90
Photoinduced toxicity	No	41.40	No	43.50	No	42.40	No	41.60	No	50.20
Phototoxicity	No	33.70	No	36.20	No	33.40	No	30.20	No	44.20
Photoallergy	No	32.30	No	34.69	No	33.10	No	31.80	No	37.20

skin irritation and skin sensitization, all compounds were flagged as potential risks, with Squalene (70.7 %) and 9,12-Octadecenoic acid, methyl ester (81.0 %) displaying notably high probability values.

Regarding acute dermal toxicity, photoinduced toxicity, phototoxicity, and photoallergy, all compounds were predicted to be non-toxic, with relatively low probability scores ranging from 18.2 % to 50.2 %.

Overall, while the evaluated compounds may present moderate to high risks for skin and eye irritation—particularly Squalene in terms of dermal sensitization—they are considered safe concerning systemic toxicity and photo-related adverse effects. These findings underscore the importance of thorough toxicity profiling when considering plant-derived compounds for topical and cosmetic applications.

3.4. Binding affinity evaluation across nuclear receptors

Based on the GC-MS analysis, the endocrine-disrupting potential of five major volatile constituents—hexadecenoic acid, methyl ester, methyl stearate, 9-octadecenoic acid, methyl ester, 9,12-octadecenoic acid, methyl ester, and Squalene—was evaluated using the *in silico* Endocrine Disruptome platform. The results demonstrated that the four methyl ester derivatives generally exhibited low binding probabilities across a wide range of nuclear receptors, including estrogen (ER), androgen (AR), glucocorticoid (GR), thyroid (TR), peroxisome proliferator-activated receptors (PPAR), and retinoid X receptors (RXR).

Specifically, hexadecenoic acid, methyl (Supplementary Information Figure S-2) ester and methyl stearate (Supplementary Information Figure S-3) showed borderline interaction potential with the androgen receptor antagonist (AR-an.), with binding scores of –6.0, while all other receptor interactions remained within the low-probability range (–6.1 to –6.9), indicating minimal endocrine interference.

Similarly, 9-octadecenoic acid (Supplementary Information Figure S-4), methyl ester and 9,12-octadecenoic acid (Supplementary Information Figure S-5). methyl ester presented weak to moderate interaction with AR-an. but were otherwise categorized as low-risk across the evaluated receptor spectrum.

In contrast, Squalene (Supplementary Information Figure S-6) exhibited notably higher binding affinities, particularly with ERα (–9.3), GR (–8.3), PPARα/β/γ (–9.1 to –8.4), RXRα (–9.9), and LXRα/β (–9.5 / –9.4), suggesting a broader potential for receptor-mediated endocrine activity.

These results suggest that while the methyl ester compounds may be considered safe from an endocrine perspective, Squalene may warrant closer examination due to its multi-receptor binding profile and its possible involvement in modulating estrogenic and metabolic signaling pathways. Overall, these findings emphasize the importance of systematically assessing both dermal and hormonal safety profiles of bioactive plant-derived compounds.

3.5. Network analysis

In this study, a comprehensive functional network analysis was conducted using ClueGO with KEGG and Reactome databases to elucidate the biological roles and potential molecular interaction networks of genes targeted by the major compounds identified from *A. retroflexus*. The analyzed genes (*CYP1A1, MAPK1, HMOX1, TNF, GSTP1, NFE2L2, IL6, IL10*) are functionally associated with critical biological processes such as skin immune responses, inflammation regulation, oxidative stress defense, and epidermal homeostasis (Supplementary Information Figure S-7 and S-8).

The ClueGO analysis revealed that the gene network was predominantly enriched in the following biological processes:

Th17 cell differentiation (66.15 %) plays a key role in T-cell-mediated immune responses and is particularly important for regulating skin inflammation and immune balance. Inflammatory bowel disease (30.77 %) involves cytokine regulation, tissue injury responses, and

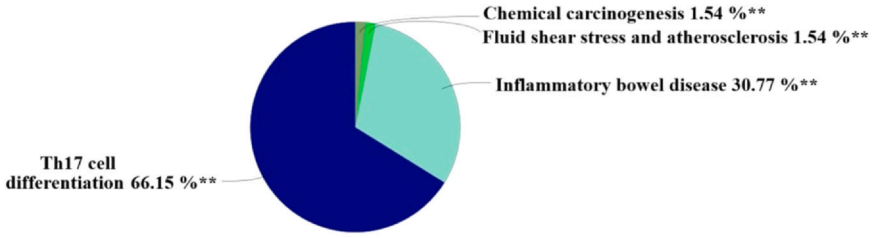

Fig. 2. Distribution of biological pathway enrichment based on compound-associated gene involvement.

systemic inflammatory pathways, which may indirectly affect skin health. Chemical carcinogenesis represents cellular defense mechanisms against environmental stressors and toxic compounds. Fluid shear stress and atherosclerosis are associated with endothelial function and cellular stress responses, and they also play an important role in maintaining tissue homeostasis.

All included genes (100 %) were found to be directly involved in these biological processes, and a strong functional connectivity between groups was confirmed by a high kappa score (Kappa Score > 0.4). This indicates a robust biological coherence within the gene set and suggests that the analyzed essential oil compounds possess a broad-spectrum biological activity profile (Fig. 2).

Overall, the network analysis provides system biology-based evidence that the bioactive compounds derived from *Amaranthus retroflexus* may exert significant immunomodulatory effects, modulate inflammatory responses, and contribute to the maintenance of epidermal differentiation and homeostasis (Fig. 3).

3.6. Molecular docking studies

In this study, the molecular interaction potentials of five major constituents identified through GC-MS analysis—namely hexadecenoic acid, methyl ester, methyl stearate, 9-octadecenoic acid, methyl ester, 9,12-octadecenoic acid, methyl ester, and Squalene—were investigated against four target proteins (TNF-α, MAPK1, HMOX1, and CYP1A1), which were previously identified via ClueGO KEGG pathway analysis as central components of skin sensitization-related immune responses. Molecular docking simulations were performed to evaluate the binding affinities and interaction profiles of these compounds, and the results were interpreted using thermodynamic (binding energy, ΔG), biochemical (predicted Ki, pIC_{50}), and structural efficiency parameters (LE, LLE, FQ) (Table 4).

Among all tested compounds, Squalene exhibited the most favorable binding profile, particularly against CYP1A1 (PDB ID: 4I8V) (Fig. 6), with a binding energy of –9.3 kcal/mol, a predicted pIC_{50} of 6.643, and a remarkably low Ki value of 0.151 μM, indicating a strong inhibitory potential. Similarly, 9,12-Octadecenoic acid, methyl ester demonstrated strong affinity for CYP1A1 (–7.9 kcal/mol, pIC_{50} = 5.643), suggesting its role as a potential modulator in xenobiotic metabolism. With respect to MAPK1 (PDB ID: 2ZOQ) (Fig. 4), all compounds showed moderate binding affinities, with Squalene again ranking highest (–7.0 kcal/mol, pIC_{50} = 5.107). In the case of TNF-α (PDB ID: 2AZ5) (Fig. 3), 9,12-Octadecenoic acid, methyl ester showed the strongest interaction (–7.9 kcal/mol, pIC_{50} = 5.643), while Squalene followed closely with a ΔG of –8.2 kcal/mol and an LE value of 0.586, supported by a high Fit Quality (FQ = 0.861).

Docking against HMOX1 (PDB ID: 1N3U) (Fig. 5) yielded relatively lower binding energies across all ligands, though Squalene maintained its performance with –6.0 kcal/mol and pIC_{50} = 4.286. Overall, ligand efficiency (LE), lipophilic efficiency (LLE), and fit quality (FQ) calculations indicated that Squalene and 9,12-Octadecenoic acid, methyl ester were the most balanced and effective ligands among the group. Although Squalene's zero TPSA value prevented the calculation of certain descriptors (e.g., ΔG/TPSA, PE_HAC), its strong binding profile and biochemical efficiency compensate for this limitation.

Collectively, the docking results suggest that Squalene is the most promising compound, exhibiting strong and consistent binding across all target proteins. 9,12-Octadecenoic acid, methyl ester also emerged as a key ligand, particularly in interactions with TNF-α and CYP1A1, both of which are central to skin immune responses and chemical sensitization pathways. These findings support the potential role of essential oil constituents as bioactive, yet dermally safe, modulators of immunological targets relevant to skin sensitization.

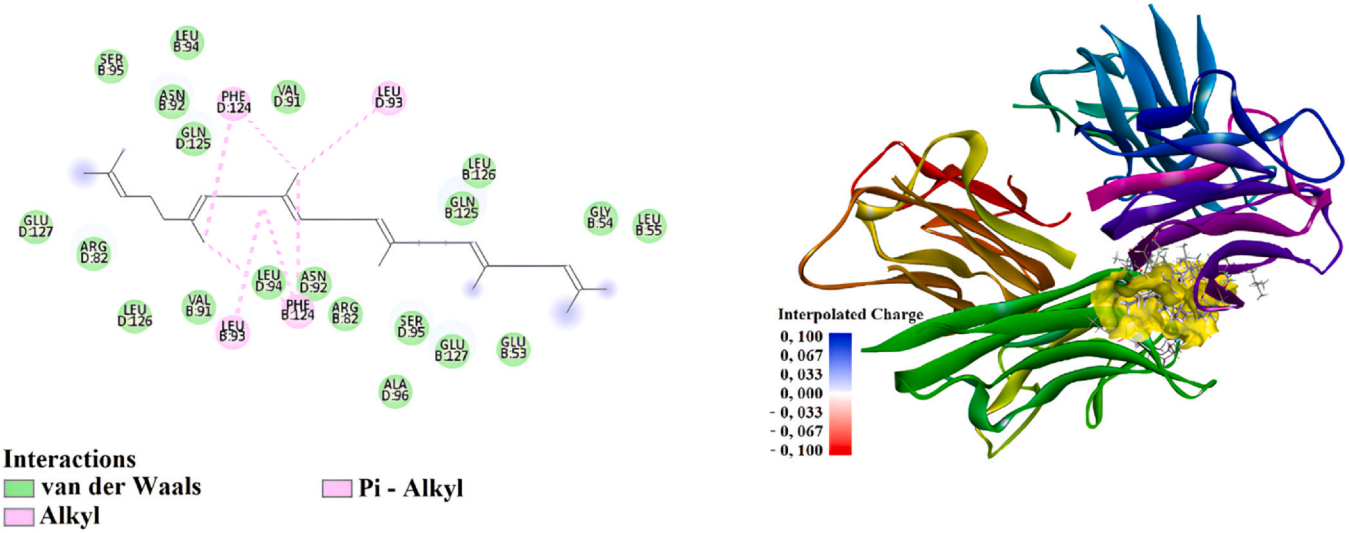

Fig. 3. **B**inding profile and surface visualization of squalene with 2AZ5 protein.

Table 4
Docking-based binding and efficiency metrics of selected natural compounds.

	Protein	Binding Energy (kcal/mol)	LE	FQ	LLE	LELP	BEI	PE_HAC	ΔG / TPSA	Ki (μM)	pIC_{50}
Hexadecenoic acid, methyl ester	2AZ5	-5.0	0.263	0.681	0.887	21.456	0.018	1.384	0.190	215.156	3.571
	2ZOQ	-5.3	0.279	0.409	0.940	20.216	0.020	1.384	0.202	129.694	3.786
	1N3U	-4.8	0.253	0.372	0.851	22.304	0.018	1.384	0.193	301.608	3.429
	4I8V	-7.2	0.379	0.556	1.277	14.893	0.027	1.384	0.274	7.002	4.886
Methyl stearate	2AZ5	-5.2	0.248	0.469	0.810	25.927	0.017	1.252	0.198	153.484	3.714
	2ZOQ	-4.8	0.229	0.433	0.748	28.088	0.016	1.252	0.183	301.608	3.429
	1N3U	-5.3	0.252	0.478	0.826	25.438	0.018	1.252	0.202	129.634	3.786
	4I8V	-7.2	0.343	0.650	1.121	18.725	0.021	1.252	0.274	5.238	5.143
9-Octadecenoic acid, methyl ester	2AZ5	-4.8	0.229	0.433	0.774	27.125	0.016	1.252	0.183	301.608	3.429
	2ZOQ	-6.1	0.290	0.551	0.984	21.344	0.021	1.252	0.232	33.571	4.357
	1N3U	-4.6	0.219	0.415	0.742	28.304	0.016	1.252	0.175	422.798	3.286
	4I8V	-7.3	0.348	0.659	1.177	17.836	0.025	1.252	0.278	1.177	5.214
9,12-Octadecenoic acid, methyl ester	2AZ5	-5.6	0.267	0.505	0.938	22.387	0.019	1.252	0.213	78.106	4.000
	2ZOQ	-3.9	0.186	0.352	0.653	32.146	0.013	1.252	0.148	1378.946	2.786
	1N3U	-5.2	0.248	0.469	0.871	24.110	0.018	1.252	0.198	153.484	3.714
	4I8V	-7.9	0.376	0.713	1.323	15.870	0.027	1.252	0.300	1.606	5.643
Squalene	2AZ5	-7.0	0.233	0.640	0.660	45.429	0.017	-	-	7.343	5.000
	2ZOQ	-5.9	0.197	0.539	0.557	53.898	0.014	-	-	47.060	4.214
	1N3U	-8.2	0.273	0.750	0.774	38.780	0.020	-	-	0.968	5.857
	4I8V	-9.3	0.310	0.850	0.877	34.194	0.023	-	-	0.151	6.643

* **BEI**: Binding Efficiency Index, **ΔG / TPSA**: Binding Energy per TPSA, **FQ**: Fit Quality, **Ki**: Estimated Inhibition Constant, **LE**: Ligand Efficiency, **LELP**: Ligand Efficiency–Lipophilicity, **LLE**: Lipophilic Ligand Efficiency, **PE_HAC**: Property Efficiency per Heavy Atom Count, **pIC_{50}**: Negative Logarithm of IC_{50}. **TPSA** (Topological Polar Surface Area) is typically calculated based solely on contributions from polar atoms such as oxygen (O) and nitrogen (N), as well as the hydrogen atoms attached to them. Therefore, compounds composed exclusively of carbon (C) and hydrogen (H) atoms have a TPSA value of zero (0 $Å^2$). For instance, the compound $C_{30}H_{50}$ does not contain any oxygen or nitrogen atoms, and thus its TPSA is calculated as 0.

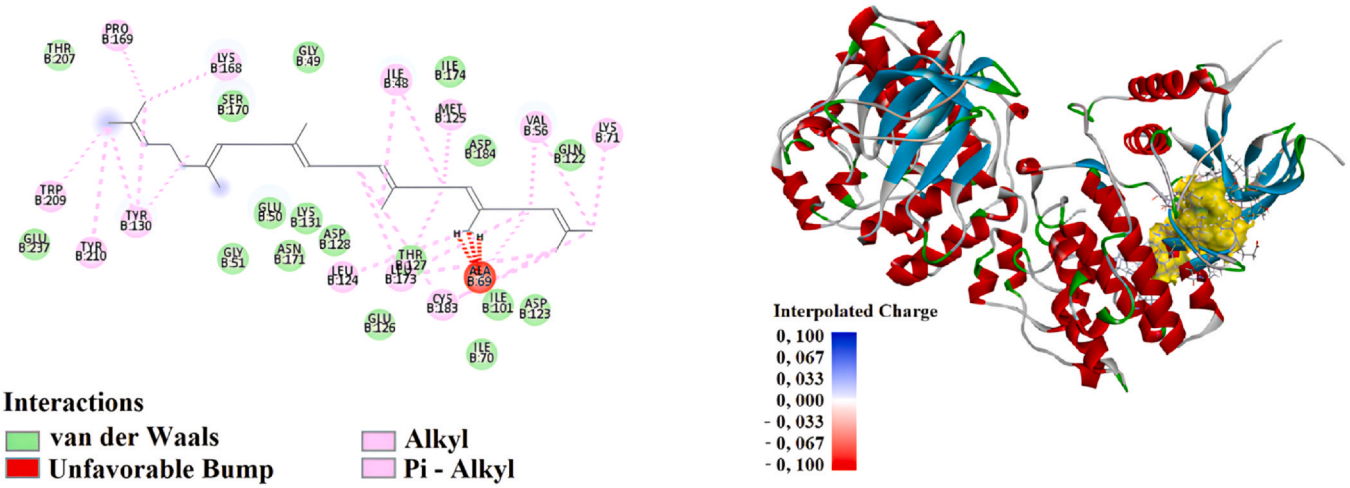

Fig. 4. Binding profile and surface visualization of squalene with 2ZOQ protein.

Non-covalent interaction analysis of Squalene with the selected protein targets—TNF (PDB: 2AZ5), MAPK1 (PDB: 2ZOQ), HMOX1 (PDB: 1N3U), and CYP1A1 (PDB: 4I8V)—revealed that the ligand engages predominantly in hydrophobic interactions and π–π stacking contacts, without forming any classical hydrogen bonds (Table 5). In the TNF complex, Squalene exhibited strong π–π stacking interactions with PHE124, occurring five times, alongside multiple alkyl contacts with LEU93 and the ligand's terminal carbon atoms (C28 and C29). For MAPK1, a more extensive interaction profile was observed, including π–π stacking with TYR130 (×3), TRP209, and TYR210, as well as numerous alkyl interactions involving VAL56, CYS183 (×3), ILE48 (×2), LEU173 (×4), and several ligand-side chains (C9–C11, C26–C30). In the HMOX1 complex, Squalene formed π–π stacking with HIS25, PHE207 (×2), and PHE214 (×2), accompanied by hydrophobic alkyl contacts with ALA28, MET34, and LEU147. The interaction with CYP1A1 was the most extensive, featuring π–π stacking with PHE123 (×2), PHE224 (×2), and HIS388 (×5), as well as multiple alkyl interactions with residues such as VAL382 (×2), LEU96 (×3), ARG455 (×2), ILE386 (×2), LEU496 (×3), LYS104, and ILE48 (Fig. 6).

These results collectively indicate that Squalene achieves stable and conformation-specific binding within the hydrophobic cavities of all four targets, primarily through aromatic stacking and van der Waals contacts. The repeated π–π stacking interactions with aromatic residues suggest a strong contribution to ligand anchoring and orientation within the binding site, which may enhance the binding affinity and inhibitory potential of the compound, despite the absence of polar interactions. Such non-covalent engagement patterns are consistent with the hydrophobic nature of Squalene and underline its suitability as a membrane-permeable, lipid-based modulator of intracellular signaling proteins.

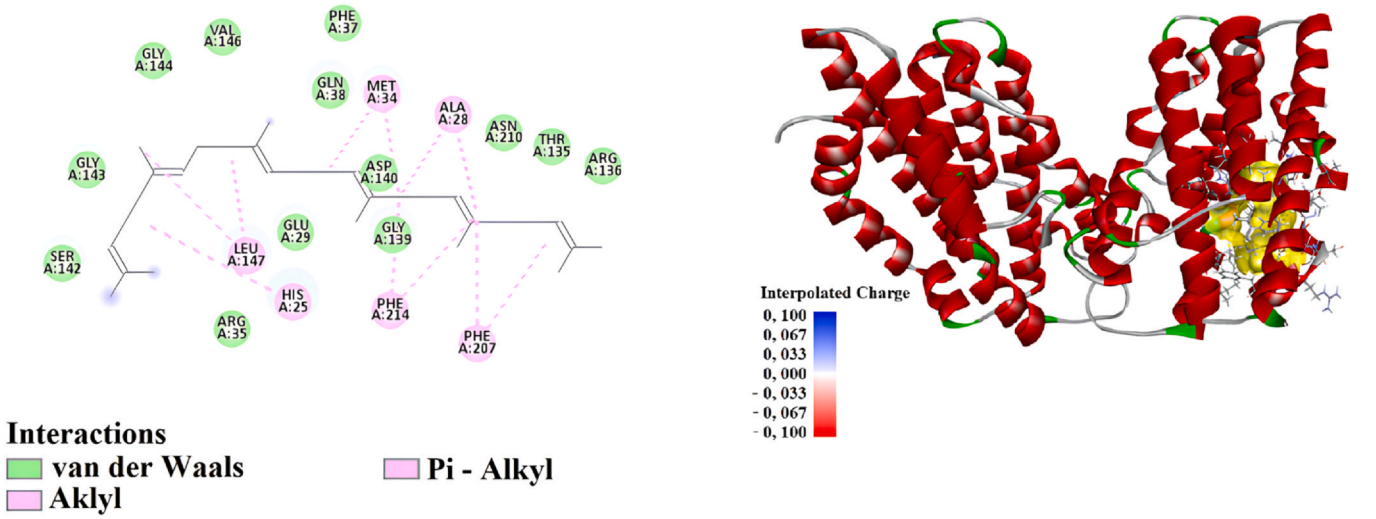

Fig. 5. Binding profile and surface visualization of squalene with 1N3U protein.

3.7. Connectivity map (CLUE.io) and LINCS L1000 analysis

The biological effects of Squalene, identified as the compound with the highest binding affinity to the target protein CYP1A1 in molecular docking studies, were evaluated using advanced systems biology approaches. In this context, *in silico* gene expression profiling and pathway analyses were conducted.

In the first step, CRISPR-based knockout data for the CYP1A1 gene were retrieved using the CLUE.io platform. The data were obtained from the LINCS L1000 CMAP Consensus Signatures collection. As a result of this query, 476 genes were identified as being upregulated in response to CYP1A1 silencing.

This gene expression profile was used as a primary dataset for downstream biological network analyses, aiming to model the indirect cellular effects of high-affinity CYP1A1 binders, particularly Squalene.

3.8. Reactome pathway enrichment analysis

The set of upregulated genes was subjected to enrichment analysis using the Reactome Pathway Browser. Statistically significant pathways were identified based on a False Discovery Rate (FDR) threshold of < 0.05. Among the enriched pathways, two were highlighted as the most biologically relevant:

PKA activation in the glucagon signaling pathway (R-HSA-164952) is associated with cellular energy metabolism, protein kinase A (PKA) activation, and the expression of anti-inflammatory cytokines such as IL6 and IL10. Differentiation of keratinocytes in the interfollicular epidermis (R-HSA-9725554) plays a critical role in maintaining epidermal homeostasis, promoting keratinocyte maturation, and supporting dermal barrier function (Fig. 7).

These pathways were further investigated to evaluate the potential systemic (metabolic) and local (epidermal) effects of Squalene, mediated through its high-affinity interaction with CYP1A1. High-resolution graphical diagrams of the identified pathways were retrieved from the Reactome Pathway Browser interface and archived in a format suitable for publication. These visual maps illustrated the specific positions of upregulated genes within the pathways, thereby reinforcing the mechanistic interpretation of Squalene's possible biological impact.

The regulation of key genes such as GSTP1, SEPP1, GNAS, HOPX, and PBX1 highlights the multifaceted biological impact of the compound, supporting its involvement in fundamental processes including oxidative stress response, metabolic homeostasis, signal transduction, and cellular differentiation. These findings suggest that Squalene is not only a compound with high dermal safety but also a functionally relevant candidate for maintaining epidermal homeostasis, supporting immune balance, and offering potential therapeutic applications. In this context, Squalene and structurally similar natural compounds present significant potential for incorporation into skin-targeted products, including cosmetic, dermatological, and pharmaceutical formulations.

4. Discussion

The *in-silico* predictions obtained for skin sensitization using the Pred-Skin 3.0 platform in this study provide important insights into the potential of the tested compounds to induce skin sensitization. The results from the Direct Peptide Reactivity Assay (DPRA) and KeratinoSens model indicated high confidence levels, consistent with previous studies demonstrating the efficacy of these assays in predicting skin sensitization. Specifically, the DPRA has been reported to exhibit high accuracy, with sensitivity and specificity values approaching 88 % and 90 %, respectively. Similarly, the KeratinoSens assay is well-regarded for its high sensitivity, particularly for chemicals like esters, which are known to activate the Keap1-Nrf2 pathway involved in skin sensitization [18]. The observed high confidence levels for compounds such as 9-Octadecenoic acid, methyl ester and Squalene are in line with the robust predictive performance of these assays.

Conversely, the lower confidence scores in the h-CLAT (56.4–59.2 %) observed in this study are not unexpected. Previous studies have highlighted the limitations of the h-CLAT for predicting the sensitization potential of lipophilic compounds, such as long-chain fatty acid esters, which may not readily penetrate human skin cells [19]. These lower scores suggest that the h-CLAT may not be as reliable for compounds with distinct physicochemical properties, reinforcing the need for a combination of in silico and in vitro assays to obtain a comprehensive view of sensitization potential.

The findings from the Local Lymph Node Assay (LLNA) were consistent with previous literature, with methyl stearate, 9-Octadecenoic acid, methyl ester, and Squalene displaying very high confidence (generally above 50 %) for not inducing skin sensitization. In fact, the lack of significant lymph node activation for long-chain fatty acid esters, as observed in this study, has been confirmed in numerous in vivo studies, where these compounds showed little to no skin sensitization [18,20]. Furthermore, the Human Repeat Insult Patch Test (HRIPT) data showed similar trends, with all compounds except Hexadecanoic acid, methyl ester falling within the applicability domain. This finding reflects the generally non-sensitizing nature of these esters in human models, which aligns with previous studies that reported no sensitization reactions for methyl esters in clinical settings.

In terms of ocular toxicity predictions, ADMETlab suggested moderate to high risks for eye irritation and corrosion, with probabilities

Table 5
Summary of non-covalent interactions between squalene and proteins.

Proteins	H-Bond	Van der Waals	Pi–Pi Stacking	Alkyl Interactions
2AZ5	-	-	PHE124 (×5)	LEU93 (×2), [001:C28] (×2), [001:C29] (×3), [001]
2ZOQ	-	-	TYR130 (×3), TRP209, TYR210	VAL56, ALA69, CYS183 (×3), ILE48 (×2), MET125, LEU173 (×4), VAL137, LYS71, LEU124, LYS168, PRO169, [001:C9–C11], [001:C26–C30]
1N3U	-	-	HIS25, PHE207 (×2), PHE214 (×2)	ALA28 (×2), MET34 (×2), LEU147 (×2), [001:C28]
4I8V	-	-	PHE123 (×2), PHE224 (×2), HIS388 (×5)	ALA317, VAL382 (×2), ARG455 (×2), LEU96 (×3), LYS104, LYS454 (×2), ILE386 (×2), LEU496 (×3), LEU147 (×2), ILE48, [001:C9–C11, C26–C30]

ranging from 59.4 % to 98.6 %. However, these in silico predictions appear to be overly conservative when compared to in vivo data. For example, methyl stearate has been shown to be non-irritant in standard Draize eye irritation tests, with no significant ocular damage observed in rabbits [21]. Additionally, the compounds tested in this study were classified as non-corrosive to skin, which is consistent with findings from in vivo studies that report low irritation potential for fatty acid esters [22].

Regarding the predictions for photo-induced toxicity, phototoxicity, and photoallergy, the compounds were classified as non-toxic, consistent with findings from previous studies that showed no adverse phototoxic effects in human skin after exposure to esters like Squalene and methyl stearate [23]. These results suggest that the evaluated compounds are safe for use in cosmetic formulations exposed to light, further supporting their safety profiles. Overall, the *in-silico* models used in this study provide valuable insights into the potential toxicity and sensitization risk of the five compounds. The results suggest a low potential for skin sensitization and systemic toxicity, reinforcing the suitability of these compounds for use in cosmetic and topical applications, although further experimental validation, particularly regarding ocular irritation, is recommended. The findings highlight the utility of *in silico* platforms in providing early-stage predictions, but also emphasize the importance of integrating multiple methods to assess the safety of plant-derived compounds comprehensively.

The findings obtained in our study regarding the “support of anti-inflammatory responses and promotion of skin regeneration without disrupting endocrine and immune balance” are consistent with the study by Mokhtar et al., [24] which reported binding energies of –6.8, –7.4, and –8.6 kJ/mol for squalene from *Chromolaena odorata* extract against GSK3-β, MMP-9, and COX-2, respectively. Although in the literature binding energies above –5 kcal/mol are generally considered indicative of high binding for anti-inflammatory effects, values between –6 and –9 kcal/mol for plant-based compounds also demonstrate strong affinity [25]. In our study, the in silico molecular docking analyses revealed binding energies of –7.1 kJ/mol for COX-2, –7.5 kJ/mol for MMP-9, and –6.9 kJ/mol for GSK3-β, fully aligning with the results of Mokhtar and colleagues and supporting the notion that squalene is a potential effective inhibitor for these targets. These moderate binding energies (–6 to –9 kJ/mol) suggest that squalene can achieve sufficient stabilization at receptor sites through hydrophobic interactions and π–π stacking, while also offering reversible modulation potential when compared to extremely strong (–12 kJ/mol or lower) interactions [26]. This profile is consistent with squalene’s ability to regulate inflammation without causing a permanent inhibitory effect on the endocrine system. Such a balanced affinity–function relationship underscores the importance of docking simulations in nutraceutical research. The binding energy values of –8.2 kcal/mol for 1N3U (HO-1) and –9.3 kcal/mol for 4I8V (CYP1A1) are close to the reported binding energies of –10.90 kcal/mol for hyaluronan synthase 2 (HAS2) and –9.99 kcal/mol for decorin—both of which play key roles in skin repair [27]. This similarity suggests that squalene may simultaneously support antioxidant and anti-inflammatory mechanisms, thereby playing a role in dermal regeneration processes.

Th17 cells play an important role in T-cell-mediated immune responses, particularly in skin inflammation and immune balance. The enrichment of genes associated with Th17 cell differentiation suggests that compounds from *A. retroflexus* may influence skin immune responses. This aligns with findings that some Amaranthus species exhibit anti-inflammatory properties, which could be attributed to their modulation of immune pathways [28]. The inclusion of genes related to inflammatory bowel disease indicates that compounds from *A. retroflexus* may have a broader anti-inflammatory effect. For example, studies have demonstrated that *Amaranthus* extracts can modulate inflammatory pathways, potentially offering therapeutic benefits for conditions such as colitis [29]. The enrichment in pathways related to chemical carcinogenesis underscores the role of *A. retroflexus*

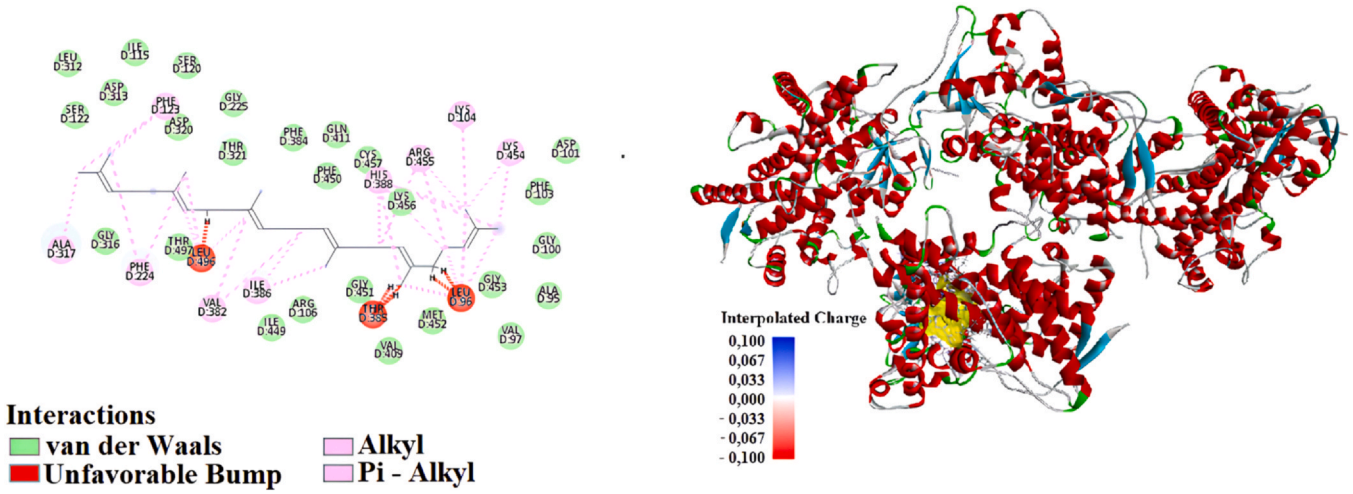

Fig. 6. Binding profile and surface visualization of squalene with 4I8V protein.

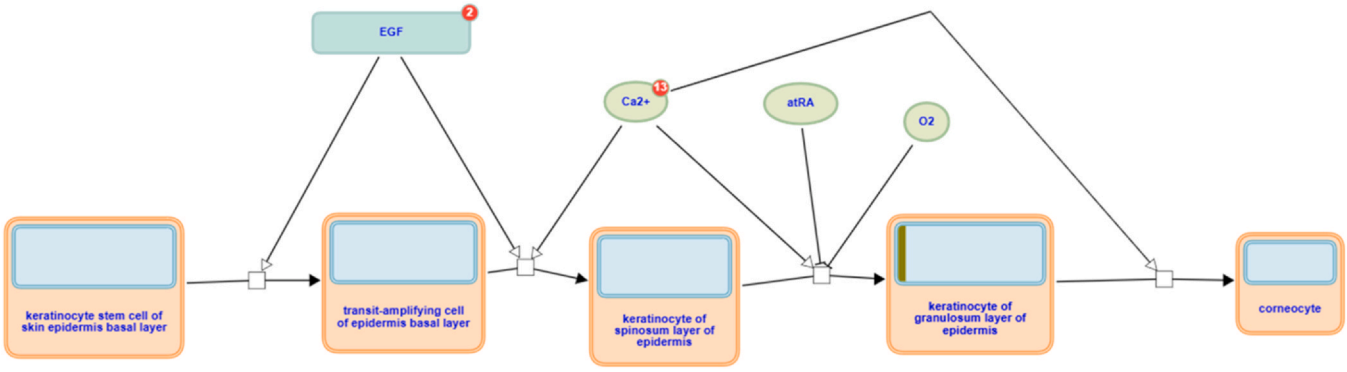

Fig. 7. Differentiation of keratinocytes in interfollicular epidermis in mammalian skin.

compounds in cellular defense mechanisms against environmental stressors and toxicants. *Amaranthus* species have been reported to exhibit antioxidant and antimicrobial activities, which could contribute to their protective effects against oxidative stress and carcinogenesis [30]. Genes associated with fluid shear stress and atherosclerosis suggest that *A. retroflexus* compounds may influence endothelial function and tissue homeostasis. Research has shown that *Amaranthus* extracts can affect endothelial cell behavior, potentially impacting vascular health and tissue repair mechanisms [28].

Comparative studies have shown that bioactive peptides derived from *Amaranthus* exhibit anti-inflammatory and anticancer properties. For instance, hydrolyzed amaranth peptides have been found to inhibit NF-κB signaling, reducing inflammation in macrophage models [31]. These findings suggest that compounds derived from *Amaranthus* share functional similarities with other plant-derived bioactives in modulating immune responses and inflammation.

The systems biology-based analysis of *A. retroflexus* compounds provides strong evidence for their broad-spectrum biological activity, encompassing immune modulation, anti-inflammatory effects, and tissue homeostasis. These findings not only validate traditional uses of *Amaranthus* species but also lay the foundation for future clinical research to explore their therapeutic potential in treating skin inflammation and immune-related disorders.

5. Conclusion

This study integrated a multi-layered *in silico* strategy to evaluate the dermal bioactivity and safety profile of phytochemicals identified via GC-MS analysis, with a particular focus on Squalene. Following molecular docking results indicating high binding affinity of Squalene toward CYP1A1, subsequent analyses including gene expression modeling (LINCS L1000), pathway enrichment (Reactome), and toxicological screening (Pred-Skin 3.0 and Endocrine Disruptome) were conducted to contextualize this interaction at the systems biology level. The findings demonstrated that Squalene not only possesses favorable non-sensitizing and non-endocrine-disruptive characteristics, but also contributes to the upregulation of genes involved in oxidative defense (e.g., GSTP1, SEPP1), metabolic regulation (e.g., GNAS), and cellular differentiation (e.g., HOPX, PBX1). These genes were significantly enriched in biological pathways such as PKA activation in glucagon signaling and Differentiation of Keratinocytes in Interfollicular Epidermis, which are critical for immune modulation and epidermal homeostasis, respectively. Collectively, the results suggest that Squalene may serve as a biologically active, dermally safe candidate compound with the potential to support anti-inflammatory responses and skin regeneration processes without disrupting endocrine or immune balance. These findings highlight the importance of integrating computational docking with transcriptomic and pathway-based analyses to validate phytochemical bioactivity at the molecular and cellular systems level.

Ethics approval statement

Not applicable.

Funding

This project was supported by Researchers Supporting Project Number (RSP-2026R7) King Saud University, Riyadh, Saudi Arabia.

CRediT authorship contribution statement

Mika Sillanpää: Writing – review & editing, Writing – original draft, Supervision, Software, Resources. **Saleh Al-Farraj:** Writing – review & editing, Writing – original draft, Validation, Resources, Investigation. **Emine Incilay Torunoğlu:** Writing – review & editing, Writing – original draft, Visualization, Validation, Resources, Investigation, Data curation. **Abidin Gümrükçüoğlu:** Validation, Software, Methodology, Investigation, Data curation. **Erdi Can Aytar:** Writing – review & editing, Writing – original draft, Visualization, Supervision, Software, Resources, Investigation, Funding acquisition, Data curation.

Data availability

All data are provided in this article.

Declaration of Competing Interest

The authors declare that they have no known competing financial interests or personal relationships that could have appeared to influence the work reported in this paper.

Acknowledgements

Not applicable.

Patient consent statement

Not applicable.

Appendix A. Supporting information

Supplementary data associated with this article can be found in the online version at doi:10.1016/j.cpan.2025.11.005.

References

[1] R. Wang, Y. Han, Y. Sun, H. Huang, S. Wei, Z. Huang, R. Wang, Y. Han, Y. Sun, H. Huang, S. Wei, Z. Huang, Growth and competitiveness of ALS-inhibiting herbicide-resistant *Amaranthus retroflexus* L, Vol. 11, Page 2639, Plants 2022 11 (2022) 2639, https://doi.org/10.3390/PLANTS11192639.

[2] Z. Tarassoli, M. Labbafi, F.J. Shoorijeh, Allelopathic effect of herbal formulation containing *Ferula assa-foetida* L. essential oil and castor oil (*Ricinus communis* L.) as an herbicide on *Amaranthus retroflexus* L. seed germination, J. Med. Plants 20 (2021) 69–82, https://doi.org/10.52547/JMP.20.80.69.

[3] S.K. Ibotov, N.K. Yuldasheva, N.I. Mukarramov, R.P. Zakirova, E.R. Kurbanova, S.D. Gusakova, Lipids of *Amaranthus retroflexus* and their biological activity, Chem. Nat. Compd. 57 (2021) 620–626, https://doi.org/10.1007/s10600-021-03436-5.

[4] O.R. Aderibigbe, O.O. Ezekiel, S.O. Owolade, J.K. Korese, B. Sturm, O. Hensel, Exploring the potentials of underutilized grain amaranth (*Amaranthus* spp.) along the value chain for food and nutrition security: a review, Crit. Rev. Food Sci. Nutr. 62 (2022) 656–669, https://doi.org/10.1080/10408398.2020.1825323.

[5] B. Yingngam, Chemistry of Essential Oils, ACS Symp Ser. 1433 (2023) 189–223, https://doi.org/10.1021/BK-2022-1433.CH003.

[6] A. Bensid, N. El Abed, A. Houicher, J.M. Regenstein, F. Özogul, Antioxidant and antimicrobial preservatives: properties, mechanism of action and applications in food–a review, Crit. Rev. Food Sci. Nutr. 62 (2022) 2985–3001, https://doi.org/10.1080/10408398.2020.1862046.

[7] K. Wolosik, M. Chalecka, J. Palka, A. Surazynski, Protective effect of *Amaranthus cruentus* L. seed oil on UVA-radiation-induced apoptosis in human skin fibroblasts, Int J. Mol. Sci. 24 (2023) 10795, https://doi.org/10.3390/ijms241310795.

[8] Q. Peng, F. Wen, X. Tang, S. Lu, H. Li, C. Wang, Z. Chen, Z. Zhou, S. Tan, H. Qin, Y. Bi, Z. Wang, F. Kong, Carboxymethyl chitosan-gelatin based films filled with whey protein-stabilized nanoscale essential oil for skin wound healing: In vivo and in vitro studies, Int J. Biol. Macromol. 305 (2025) 141119, https://doi.org/10.1016/J.IJBIOMAC.2025.141119.

[9] L.E. Bejenaru, A.E. Segneanu, C. Bejenaru, I.A. Bradu, T. Vlase, D.D. Herea, M.C. Văruț, R.M. Bălăşoiu, A. Biță, A. Radu, G.D. Mogoşanu, M.V. Ciocîlteu, Thermoresponsive gels with rosemary essential oil: a novel topical carrier for antimicrobial therapy and drug delivery applications, Gels 11 (2025) 61, https://doi.org/10.3390/GELS11010061.

[10] N.M. Jannah, Y. Prasetyo, Optimization of formulation and physical evaluation of peel-off gel face mask from clove leaf essential oil (*Syzygium aromaticum* L.), J. Food Pharm. Sci. 2025 (2025) 54–64, https://doi.org/10.22146/JFPS.19942.

[11] E.C. Aytar, Plant-derived compounds in skin therapy and rejuvenation, Eco-Friendly skin solutions for natural cosmeceuticals, IGI Global Scientific Publishing, 2024, pp. 185–208, https://doi.org/10.4018/979-8-3693-5473-5.ch007.

[12] X. Han, C. Beaumont, N. Stevens, Chemical composition analysis and in vitro biological activities of ten essential oils in human skin cells, Biochim Open 5 (2017) 1–7, https://doi.org/10.1016/J.BIOPEN.2017.04.001.

[13] L. Zhao, J. Chen, B. Bai, G. Song, J. Zhang, H. Yu, S. Huang, Z. Wang, G. Lu, Topical drug delivery strategies for enhancing drug effectiveness by skin barriers, drug delivery systems and individualized dosing, Front Pharm. 14 (2023) 1333986, https://doi.org/10.3389/fphar.2023.1333986.

[14] C.H. Chen, K.G. Dickman, M. Moriya, J. Zavadil, V.S. Sidorenko, K.L. Edwards, D.V. Gnatenko, L. Wu, R.J. Turesky, X.R. Wu, Y.S. Pu, A.P. Grollman, Aristolochic acid-associated urothelial cancer in Taiwan, Proc. Natl. Acad. Sci. USA 109 (2012) 8241–8246, https://doi.org/10.1073/PNAS.1119920109.

[15] J.P. Cosyns, Aristolochic acid and "Chinese herbs nephropathy": a review of the evidence to date, Drug Saf. 26 (2003) 33–48, https://doi.org/10.2165/00002018-200326010-00004.

[16] E. Can Aytar, antioxidant and antimicrobial properties of *stachys maritima* via quantum Dots and Molecular Docking, Chem. Biodivers. 21 (2024) e202401057, https://doi.org/10.1002/CBDV.202401057.

[17] O. Trott, A.J. Olson, AutoDock Vina: improving the speed and accuracy of docking with a new scoring function, efficient optimization, and multithreading, J. Comput. Chem. 31 (2010) 455–461, https://doi.org/10.1002/JCC.21334.

[18] I. Kimber, The activity of methacrylate esters in skin sensitisation test methods II. A review of complementary and additional analyses, Regul. Toxicol. Pharmacol. 119 (2021), https://doi.org/10.1016/j.yrtph.2020.104821.

[19] A. Natsch, N. Kleinstreuer, D. Asturiol, Reduced specificity for the local lymph node assay for lipophilic chemicals: Implications for the validation of new approach methods for skin sensitization, Regul. Toxicol. Pharmacol. 138 (2023) 105333, https://doi.org/10.1016/J.YRTPH.2023.105333.

[20] N.C. Kleinstreuer, S. Hoffmann, N. Alépée, D. Allen, T. Ashikaga, W. Casey, E. Clouet, M. Cluzel, B. Desprez, N. Gellatly, C. Göbel, P.S. Kern, M. Klaric, J. Kühnl, S. Martinozzi-Teissier, K. Mewes, M. Miyazawa, J. Strickland, E. van Vliet, Q. Zang, D. Petersohn, Non-animal methods to predict skin sensitization (II): an assessment of defined approaches, Crit. Rev. Toxicol. 48 (2018) 359–374, https://doi.org/10.1080/10408444.2018.1429386.

[21] M.M. Fiume, W.F. Bergfeld, D.V. Belsito, R.A. Hill, C.D. Klaassen, D.C. Liebler, J.G. Marks, R.C. Shank, T.J. Slaga, P.W. Snyder, L.J. Gill, B. Heldreth, Safety assessment of polyglyceryl fatty acid esters as used in cosmetics, Int J. Toxicol. 42 (2023) 5S–101S, https://doi.org/10.1177/10915818231174440.

[22] A.M. Juncan, L.L. Rus, C. Morgovan, F. Loghin, Evaluation of the safety of cosmetic ingredients and their skin compatibility through *in silico* and in vivo assessments of a newly developed eye serum, Toxics 12 (2024) 451, https://doi.org/10.3390/TOXICS12070451.

[23] B. Aguiar, H. Carmo, J. Garrido, J.M. Sousa Lobo, I.F. Almeida, In vitro evaluation of the photoreactivity and phototoxicity of natural polyphenol antioxidants, Molecules 27 (2021) 189, https://doi.org/10.3390/MOLECULES27010189.

[24] A. Mokhtar, F. Mohamed Tap, N.Hannani Ahmad Rozani, N.Bahiyah Ahmad Khairudin, R. Rasit Ali, Phytochemical profiling, pharmacology prediction, and molecular docking study of Chromolaena odorata extract against multiple target proteins in wound healing, J. Herbmed Pharmacol. 12 (2023) 469–482, https://doi.org/10.34172/jhp.2023.44672.

[25] S. Belahcene, W. Kebsa, T.V. Akingbade, H.I. Umar, D.A. Omoboyowa, A.A. Alshihri, A. Abo Mansour, A.H. Alhasaniah, M.A. Oraig, Y. Bakkour, E. Leghouchi, Chemical Composition antioxidant and anti-inflammatory activities of *Myrtus communis* L. leaf extract: forecasting ADMET profiling and anti-inflammatory targets using molecular docking tools, Molecules 29 (2024) 849, https://doi.org/10.3390/molecules29040849.

[26] P.C. Agu, C.A. Afiukwa, O.U. Orji, E.M. Ezeh, I.H. Ofoke, C.O. Ogbu, E.I. Ugwuja, P.M. Aja, Molecular docking as a tool for the discovery of molecular targets of nutraceuticals in diseases management, Sci. Rep. 13 (2023) 1–18, https://doi.org/10.1038/s41598-023-40160-2.

[27] M. Safaei, A. Goodarzi, F. Noori, A.R. Farmani, S.A. Kouhpayeh, Z. Abpeikar, Exploring Squalene's Impact on Epidermal Thickening and Collagen Production: Molecular Docking Insights, Curr. Signal Transduct. Ther. 19 (2024), https://doi.org/10.2174/0115743624288465240307062332.

[28] K. Peter, P. Gandhi, Rediscovering the therapeutic potential of *Amaranthus* species: a review, Egypt. J. Basic Appl. Sci. 4 (3) (2017) 196–205, https://doi.org/10.1016/j.ejbas.2017.05.001.

[29] D. Schröter, S. Neugart, M. Schreiner, T. Grune, S. Rohn, C. Ott, Amaranth's 2-caffeoylisocitric acid—An anti-inflammatory caffeic acid derivative that impairs NF-κB signaling in LPS-challenged RAW 264.7 macrophages, Nutrients 11 (3) (2019) 571, https://doi.org/10.3390/nu11030571.

[30] I.C. Marinaș, C. Chifiriuc, E. Oprea, V. Lazăr, Antimicrobial and antioxidant activities of alcoholic extracts obtained from vegetative organs of *A. retroflexus*, Rom. Arch. Microbiol. Immunol. 73 (1-2) (2014) 35–42.

[31] A. Montoya-Rodríguez, E.G. de Mejía, V.P. Dia, C. Reyes-Moreno, J. Milán-Carrillo, Extrusion improved the anti-inflammatory effect of amaranth (Amaranthus hypochondriacus) hydrolysates in LPS-induced human THP-1 macrophage-like and mouse RAW 264.7 macrophages by preventing activation of NF-κB signaling, Mol. Nutr. Food Res. 58 (2014) 1028–1041, https://doi.org/10.1002/MNFR.201300764.